Application of the Eulerian Subgrid Probability Density Function Method in the Large Eddy Simulation of a Partially Premixed Swirl Flame

D. Fredrich[a], **W. P. Jones**[b] and A. J. Marquis[c]

Department of Mechanical Engineering, Imperial College London, London SW7 2AZ, UK

[a]d.fredrich15@imperial.ac.uk (*), [b]w.jones@imperial.ac.uk, [c]a.marquis@imperial.ac.uk

Keywords: Large Eddy Simulation, Subgrid PDF Method, Turbulence-Chemistry Interactions, Partially Premixed Flame, Gas Turbine Combustion

Abstract

A gas turbine model combustor is studied using Large Eddy Simulation with a transported Probability Density Function approach solved by the Eulerian stochastic field method. The chemistry is represented by a reduced methane mechanism containing 15 steps and 19 species while the subgrid scale stresses and scalar fluxes are modelled, respectively, via a dynamic Smagorinsky model and a gradient diffusion approximation. The test case comprises a partially premixed swirl flame in a complex geometry. Four stochastic fields are utilised in the simulations, which are performed for two different combustor operating conditions involving a stable and an unstable flame. Good agreement between the simulation and measurement data is shown in a comparison of mean velocity, temperature and species mass fraction profiles as well as scatter plots of the instantaneous thermochemical properties. In conclusion, the predictive capabilities of the employed Large Eddy Simulation method are successfully demonstrated in this work.

1 Introduction

The interaction between turbulence and chemistry on the small, unresolved subfilter - or subgrid - scales (sgs) presents one of the major challenges in the development of Large Eddy Simulation (LES) methods for turbulent reacting flow problems. Governed by highly nonlinear reaction rates, these so-called turbulence-chemistry interactions are represented in the

LES scalar equations via a filtered chemical source term and require extensive modelling work. An overview of different closure strategies can be found, amongst others, in a review by Pitsch (2006). In contrast to the wide majority of combustion models which are formulated for one specific flame regime only, the Eulerian subgrid Probability Density Function (PDF) method employed in this work allows for a potentially regime independent description of turbulent flames. This becomes particularly useful in the context of modern gas turbine combustion where lean, partially premixed operating conditions are utilised to effectively reduce pollutant emissions such as nitrogen oxides (NO_x) and carbon monoxide (CO). Under these conditions, parts of the flow field are governed by premixed flame propagation and finite-rate effects, i.e. auto-ignition, extinction or ignition, while other parts will display mixing controlled reactions as encountered in diffusion (non-premixed) flames. The present fully Eulerian subgrid PDF method was found to perform well in both flame regimes (Jones and Navarro-Martinez 2007, Jones and Prasad 2010, 2011) and has been successfully applied to a wide range of flow configurations in the past. It was recently extended to stratified (Brauner et al. 2016) and spray (Jones et al. 2015, Gallot-Lavallée and Jones 2016) combustion and was also employed in the simulation of an industrial gas turbine combustor (Bulat et al. 2013, 2014).

The target test case chosen for this work is the PRECCINSTA (Prediction and Control of Combustion Instabilities in Industrial Gas Turbines) burner, which provides a solid basis for the assessment of LES combustion models. The gas turbine model combustor was subject to a number of experimental (Meier et al. 2007, Steinberg et al. 2013, Caux-Brisebois et al. 2014, Oberleithner et al. 2015, Yin et al. 2017, Stöhr et al. 2017) as well as computational (Roux et al. 2005, Galpin et al. 2008, Fiorina et al. 2010, Moureau et al. 2011, Lecocq et al. 2011, Franzelli et al. 2012, Veynante and Moureau 2015, Mercier et al. 2015, Wang et al. 2016, Volpiani et al. 2017) investigations in the past. Note that all computational studies were performed using either simple chemistry involving very few species and reaction steps or tabulated chemistry based on fully premixed, laminar flame calculations. A shortened flame length caused by slightly faster combustion was observed in most simulations. Furthermore, the use of adiabatic combustion chamber walls was identified to be the cause for overestimated temperatures in the Outer Recirculation Zone (ORZ) as any heat loss occurring in the experiments

remains unaccounted for.

In this work, the PRECCINSTA model combustor is simulated by applying the flame regime independent Eulerian subgrid PDF approach with a reduced 15-step and 19 species chemical mechanism. Test cases for two different combustor operating conditions are simulated and results are compared against available experimental data with the objective of evaluating the predictive capabilities of the employed LES method in the context of partially premixed combustion in a complex geometry. This includes characterisation of the flow field using mean axial and radial velocity component profiles at different locations in the combustion chamber as well as a description of the flame based on both mean and Root Mean Square (RMS) temperature, carbon dioxide (CO_2) and methane (CH_4) profiles. The simulated mean and instantaneous flame structure is further assessed in a qualitative comparison with experimental hydroxide (OH) images. Finally, the representation of fundamental thermochemical properties is evaluated by analysis of the instantaneous temperature-mixture fraction relation.

2 Mathematical formulation

2.1 Large eddy simulation

In LES, the separation of large-scale, energetic and small-scale, dissipative turbulent motions is achieved through a spatial filtering operation over the entire flow domain where the filter width is taken to be the cube root of the local grid cell volume. In order to account for the strong density variations arising in combusting flows, additional density weighted - or Favre - filtering defined by $\widetilde{f} = \overline{\rho f}/\overline{\rho}$ can be introduced. Application of this filter to the equations of motion, i.e. mass conservation (1) and momentum conservation (2), and to the scalar transport equations (3) results in the following set of filtered equations:

$$\frac{\partial \overline{\rho}}{\partial t} + \frac{\partial \overline{\rho}\widetilde{u}_i}{\partial x_i} = 0 \tag{1}$$

$$\frac{\partial \overline{\rho}\widetilde{u}_i}{\partial t} + \frac{\partial \overline{\rho}\widetilde{u}_i\widetilde{u}_j}{\partial x_j} = -\frac{\partial \overline{p}}{\partial x_i} + \frac{\partial}{\partial x_j}\left(2\mu\widetilde{S}_{ij}\right) - \frac{\partial \tau_{ij}^{sgs}}{\partial x_j} \tag{2}$$

$$\frac{\partial \overline{\rho}\widetilde{\phi}_\alpha}{\partial t} + \frac{\partial \overline{\rho}\widetilde{u}_j\widetilde{\phi}_\alpha}{\partial x_j} = \frac{\partial}{\partial x_j}\left(\frac{\overline{\mu}}{\sigma}\frac{\partial \widetilde{\phi}_\alpha}{\partial x_j}\right) - \frac{\partial J^{sgs}_{\alpha,j}}{\partial x_j} + \overline{\rho\dot{\omega}}_\alpha \tag{3}$$

The subgrid scale stress tensor $\tau^{sgs}_{ij} = \overline{\rho}\left(\widetilde{u_i u_j} - \widetilde{u}_i\widetilde{u}_j\right)$ is determined via the Smagorinsky model (Smagorinsky 1963), which introduces a subgrid scale viscosity μ_{sgs} to mimic the diffusion process on the dissipative small-scales:

$$\mu_{sgs} = \overline{\rho}(C_s\Delta)^2||\widetilde{S}_{ij}|| \tag{4}$$

where $\widetilde{S}_{ij} = \left(\partial\widetilde{u}_i/\partial x_j + \partial\widetilde{u}_j/\partial x_i\right)/2$ and $||\widetilde{S}_{ij}|| \equiv \left(2\widetilde{S}_{ij}\widetilde{S}_{ij}\right)^{1/2}$ are the resolved rate of strain tensor and its respective Frobenius norm. The Smagorinsky parameter C_s is obtained through the dynamic procedure of Piomelli and Liu (1995). The isotropic part of the viscous and subgrid scale stresses is absorbed into the pressure. Based on a Lewis number unity assumption (Poinsot and Veynante 2005), the scalar transport equations (3) are expressed in terms of a general scalar $\phi_\alpha = [\phi_1, ..., \phi_{N_s}]$ representing the species mass fractions Y_α and the enthalpy h where N_s is the number of scalars required to describe the system, i.e. species plus enthalpy. A low-Mach-number flow, constant thermodynamic pressure and equal diffusivities for all species $D_\alpha = D$, which can be related to the viscosity via the Prandtl - or Schmidt - number $\sigma = \mu/\rho D$, have been assumed in the formulation. A gradient diffusion approximation is adopted for the scalar fluxes $J^{sgs}_{\alpha,j}$ (Schmidt and Schumann 1989). The filtered chemical source term representing the net rate of species formation through chemical reaction $\overline{\rho\dot{\omega}}_\alpha$ remains unclosed and requires modelling.

2.2 Eulerian subgrid PDF method

The combustion model underlying the present work is a fully Eulerian transported subgrid PDF approach. Following Gao and O'Brien (1993) and through the application of Favre filtering, a joint subgrid PDF can be derived according to:

$$\widetilde{P}_{sgs}(\underline{\psi}; \mathbf{x}, t) = \frac{1}{\overline{\rho}}\int_\Omega \rho G(\mathbf{x} - \mathbf{x}', \Delta(\mathbf{x}))\mathscr{F}(\underline{\psi}; \mathbf{x}', t)\mathrm{d}\mathbf{x}' \tag{5}$$

Here, $\mathscr{F}$ denotes the joint PDF, which is the product of the fine-grained probability density function P_α of each reactive scalar:

$$\mathscr{F}(\underline{\psi};\mathbf{x},t) = \prod_{\alpha=1}^{N_s} P_\alpha = \prod_{\alpha=1}^{N_s} \delta\left[\psi_\alpha - \phi_\alpha(\mathbf{x},t)\right] \tag{6}$$

where ψ_α is the sample - or composition - space of the reactive scalar ϕ_α and δ is the Dirac-function. An exact equation describing the evolution of $\widetilde{P}_{sgs}$ can be derived from the appropriate conservation equations using standard methods, e.g. Gao and O'Brien (1993). This formulation contains the chemical reaction term (I), which appears in closed form, as well as two additional unknown terms representing subgrid scale convection (II) and molecular diffusion (III) of the PDF. In the present work, these unknown terms are approximated by a gradient closure directly analogous to the LES Smagorinsky model and by the Linear Mean Square Estimation (LMSE) closure (Dopazo and O'Brien 1974), respectively. Taking into account the approach of Brauner et al. (2016), the subgrid PDF evolution equation appears in its final form:

$$\begin{aligned}\overline{\rho}\frac{\partial \widetilde{P}_{sgs}(\underline{\psi})}{\partial t} + \overline{\rho}\widetilde{u}_j\frac{\partial \widetilde{P}_{sgs}(\underline{\psi})}{\partial x_j} &= \underbrace{\sum_{\alpha=1}^{N_s}\frac{\partial}{\partial \psi_\alpha}\left[\overline{\rho}\dot{\omega}_\alpha(\underline{\psi})\widetilde{P}_{sgs}(\underline{\psi})\right]}_{\textbf{I:}\text{ closed chemical reaction term}} \\ \underbrace{+\frac{\partial}{\partial x_j}\left[\left(\frac{\mu}{\sigma}+\frac{\mu_{sgs}}{\sigma_{sgs}}\right)\frac{\partial \widetilde{P}_{sgs}(\underline{\psi})}{\partial x_j}\right]}_{\textbf{II:}\text{ sgs convection term (gradient closure)}} &\underbrace{-\frac{C_d}{2\tau_{sgs}}\sum_{\alpha=1}^{N_s}\frac{\partial}{\partial \psi_\alpha}\left[\overline{\rho}(\psi_\alpha - \widetilde{\phi}_\alpha(\mathbf{x},t))\widetilde{P}_{sgs}(\underline{\psi})\right]}_{\textbf{III:}\text{ molecular diffusion term (LMSE closure)}}\end{aligned} \tag{7}$$

Here, the values 0.7 and 2.0 are assigned, respectively, to the subgrid scale - or turbulent - Schmidt number σ_{sgs} and the micro-mixing constant C_d. The micro-mixing time scale τ_{sgs} is assumed to be given by:

$$\tau_{sgs} = \frac{\overline{\rho}\Delta^2}{\mu_{sgs}}\left(1 - \exp\left(-\mathscr{R}^2\right)\right) \tag{8}$$

with a subgrid scale turbulence Reynolds number defined as $\mathscr{R} = \mu_{sgs}/\mu$.

The Eulerian stochastic field method is used to solve the closed form of the subgrid PDF evolution equation (7), where $\widetilde{P}_{sgs}(\underline{\psi})$ is represented by an ensemble of N stochastic fields - namely $\xi_\alpha^n(\mathbf{x},t)$ - for each of the N_s reactive scalars. The joint subgrid PDF equation (5) can

then be rewritten as follows:

$$\widetilde{P}_{sgs}(\underline{\psi};\mathbf{x},t) = \frac{1}{N}\sum_{n=1}^{N}\frac{1}{\overline{\rho}}\int_{\Omega}\rho G(\mathbf{x}-\mathbf{x}',\Delta(\mathbf{x}))\times\prod_{\alpha=1}^{N_s}\delta\left[\psi_\alpha-\xi_\alpha^n(\mathbf{x},t)\right]\mathrm{d}\mathbf{x}' \tag{9}$$

Two approaches by Valiño (1998) and Sabel'nikov and Soulard (2005) exist for the derivation of a system of stochastic differential equations equivalent to the subgrid PDF evolution equation (7). In the present work, the Itô formulation is adopted for the stochastic integral (Valiño 1998) and the stochastic fields thus evolve according to:

$$\begin{aligned}\overline{\rho}\mathrm{d}\xi_\alpha^n+\overline{\rho}\widetilde{u}_i\frac{\partial\xi_\alpha^n}{\partial x_i}\mathrm{d}t = \overline{\rho}\dot{\omega}_\alpha^n(\underline{\xi}^n)\mathrm{d}t+\frac{\partial}{\partial x_i}\left[\Gamma'\frac{\partial\xi_\alpha^n}{\partial x_i}\right]\mathrm{d}t \\ -\frac{C_d\overline{\rho}}{2\tau_{sgs}}\left(\xi_\alpha^n-\widetilde{\phi}_\alpha\right)\mathrm{d}t+\left(2\overline{\rho}\frac{\mu_{sgs}}{\sigma_{sgs}}\right)^{1/2}\frac{\partial\xi_\alpha^n}{\partial x_i}\mathrm{d}W_i^n\end{aligned} \tag{10}$$

where $\Gamma' = \mu/\sigma + \mu_{sgs}/\sigma_{sgs}$ is the total diffusion coefficient. The Wiener process $\mathrm{d}W_i^n$ is approximated by time-step increments $\eta_i^n(\mathrm{d}t)^{1/2}$ where η_i^n is a $\{-1,1\}$ dichotomic random vector, which is different for each field but independent of the spatial location **x**. The Favre filtered value of each reactive scalar ϕ_α can finally be obtained from averaging over the stochastic fields:

$$\widetilde{\phi}_\alpha = \frac{1}{N}\sum_{n=1}^{N}\xi_\alpha^n \tag{11}$$

3 Test case

3.1 Experimental set-up

The initial experimental test campaign of the PRECCINSTA gas turbine model combustor considered in this work was conducted by Meier et al. (2007) at the DLR (German Aerospace Center). Measurements were performed for three different operating conditions by varying the fuel mass flow rate to adjust the global equivalence ratio Φ_{glob} of the mixture. An oscillating flame undergoing self-excited thermo-acoustic instabilities was observed at Φ_{glob} = 0.7 (case 1). Increasing the fuel mass flow rate to Φ_{glob} = 0.83 (case 2a) resulted in a 'quiet' flame not exhibiting any oscillations whereas Φ_{glob} = 0.75 (case 2b) produced a subtly pulsating flame.

The combustor geometry is shown schematically in Fig. 1 and comprises four sections.

Dry, pure air at atmospheric conditions is fed into the plenum section through a large orifice. The injector section consists of a radial swirler followed by a ‘bluff body’ and was derived from an industrial design by Turbomeca. In between each of the 12 swirler vanes, fuel (methane) is injected into the air stream with high momentum to ensure good mixing. The chamber section is made of 1.5 mm thick quartz glass windows with a 85 x 85 mm^2 cross section area and a total length of 114 mm. Its entry plane - aligned with tip of the ‘bluff body’ - is defined as axial location h_0 = 0 mm for all measurements. Burnt combustion products leave the domain through the exit section connecting the combustor to the atmosphere via a converging duct. Comprehensive experimental data is available from Laser Doppler Velocimetry (LDV) measurements for the cases 1 and 2b as well as laser Raman scattering measurements for the cases 1 and 2a. These provide both mean and RMS values of the velocity, temperature, mixture fraction and major species mass fractions. Measurements were performed along radial profiles in one vertical plane at different axial locations within the combustion chamber. Additional planar Laser-Induced Fluorescence (LIF) of OH radicals was applied to visualise the flame structure. An overview of the three different combustor operating conditions including the employed measurement techniques can be found in Table 1 while the systematic and statistical measurement uncertainties are presented in Table 2.

3.2 Numerical set-up

The in-house, block-structured, boundary conforming coordinate LES code BOFFIN-LES is employed to carry out the computations. It is fully parallelised by means of domain decomposition and MPI message passing routines. The code utilises a second-order-accurate finite volume method, based on a low-Mach-number, pressure based, variable density formulation. For the momentum equation convection terms, an energy-conserving discretisation scheme is used. All other spatial derivatives are discretised with second-order central differences, with the exception of the convective terms in the scalar equations. These are discretised using a Total Variation Diminishing (TVD) scheme to avoid unphysical overshoots. A description of the weak first-order temporal approximation used for solving the stochastic field equations can be found in Mustata et al. (2006).

Test cases 1 and 2a corresponding to an oscillating flame (Φ_{glob} = 0.7) and a 'quiet' flame (Φ_{glob} = 0.83) are considered in this work. Four stochastic fields are utilised to represent the influence of the subgrid scale contributions. The computational domain is almost identical to the combustor geometry investigated in the experimental test campaign. A close-up of the generated block-structured mesh containing $\sim$2.7 million cells is shown on the right-hand side of Fig. 1. In order to account for preheating of the mixture, as observed in the experiments (Meier et al., 2007), both air and methane are injected at a temperature of 320 K and a pressure of 1 bar. The inlet velocities have been adjusted accordingly to reflect the prescribed mass flow rates. A zero-gradient pressure boundary condition is adopted for the outlet plane and all domain walls are treated as adiabatic. Radiative heat transfer is included in the simulations through the radiation model described in Barlow et al. (2001). The chemistry is represented by a 15-step Augmented Reduced Mechanism (ARM) involving 19 species, which was derived by Sung et al. (2001) from the full GRI 3.0 mechanism and is listed in Table 3.

4 Results and discussion

4.1 'Quiet' flame

Results for the 'quiet' flame (Φ_{glob} = 0.83) are presented and discussed first. In order to understand the flame topology, mean and instantaneous images of the OH intensity are displayed in Fig. 2 in a strictly qualitative comparison between experiments and simulation. Generally, the LES replicates the flame structure well despite not being able to resolve the smallest turbulent length scales captured by the LIF measurements. Wrinkling of the flame front seems to increase with downstream position where most of the smaller structures are found. The flame's characteristic V-shape can be clearly identified in both studies although mismatching spreading angles of the outer flame surface lead to a reduced flame width in the simulation. Moreover, a noticeable difference in the depicted flame lengths can be determined from the mean images. The jet of low OH intensities in the experimental image extends beyond 30 mm into the combustion chamber whereas reaching only about 25 mm in the LES snapshot. An over predicted degree of premixing (described later based on Fig. 5) could potentially be the cause for the underestimated outer flame angle and length.

Figure 3 shows radial profiles of the mean and RMS temperature and CH_4 mass fraction at five different axial positions in the combustion chamber. High mean temperatures near the centreline characterise the Inner Recirculation Zone (IRZ) where burnt gases are transported back to the flame front with the purpose of stabilising the flame. These temperatures, both mean and RMS, as well as the CH_4 mass fractions in this region are in excellent agreement with experimental data. Discrepancies between the measured and simulated temperature profiles appear towards the combustion chamber walls as a result of two overlapping effects. Heat loss occuring in the experimental test campaign, also mentioned in e.g. Moureau et al. (2011), can be determined by cross-correlating the temperature and CH_4 mass fraction profiles at axial positions h_6 and h_{10}. In the region $r > 25$ mm, both the computed and measured mean and RMS values of the CH_4 mass fraction are approximately zero indicating a fully burnt mixture. The temperature deviation in this region is therefore most likely caused by experimental heat loss. Further downstream at h_{20} and h_{30}, the temperature differences become more significant and are complemented by a discrepancy in the CH_4 mass fraction profiles. Compared to measurement data, an earlier consumption of CH_4 - with downstream position - occurs and the mean temperatures converge towards their 'equilibrium' state at a quicker rate. A shortened flame length can be concluded (in agreement with the OH images in Fig. 2) as first described by Galpin et al. (2008) who argued a higher degree of premixing in their simulations leads to the increased burning rate. In accordance with the under predicted flame length, RMS temperature and CH_4 mass fraction intensities towards the combustion chamber walls are not sufficiently captured by the LES, particularly at the downstream positions. Nevertheless, a fair description of the general RMS trends can be observed. At h_{80}, all of the CH_4 is fully consumed, the temperature distribution becomes homogeneous and the RMS values become negligible as expected from the experimental measurements.

4.2 Oscillating flame

A simulation of the oscillating flame case (Φ_{glob} = 0.7) was performed to complement the 'quiet' flame results presented above. Note that the low-Mach-number solver applied in this work will not propagate acoustic waves, prohibiting the reproduction of thermo-acoustic insta-

bilities observed in the experiments (Meier et al. 2007). Radial profiles of the mean axial and radial velocity component for the oscillating flame are shown on the left-hand side of Fig. 4. Three distinctive flow regions can be identified when characterising the flow field. The conically shaped, swirling jet of unburnt gases is characterised by high axial and radial velocity magnitudes reaching approximately 40 m/s and 20 m/s, respectively. The jet transitions into an Outer Recirculation Zone (ORZ), located outside of the experimentally measured region, which can easily be detected by low velocity magnitudes towards the combustion chamber walls. High negative velocities around the combustor centreline indicate an Inner Recirculation Zone (IRZ), created by the swirling flow to stabilise the flame. The high velocity jet widens with increasing downstream position and shifts towards the combustion chamber walls reducing the size of the ORZ while widening the IRZ. Overall, the quantitative velocity results match experimental data with very high accuracy as all of the above-mentioned flow features are captured in the simulation.

The right-hand side of Fig. 4 presents radial profiles of the mean and RMS temperature. A corresponding instantaneous snapshot of the temperature field is depicted in Fig. 1 illustrating the highly turbulent flame behaviour. Looking at the mean profiles, general temperature trends including the location of the temperature dip representing unburnt gases are well reproduced by the LES. Unaccounted heat loss effects at the combustion chamber walls as well as a shortened flame length can be detected similar to the 'quiet' flame case. At h_{80} both the experimental and numerical temperatures reach a homogeneous 'equlibrium' state at the adiabatic flame temperature of just over 1800 K. From the RMS profiles, it becomes clear that temperature fluctuations towards the combustor centreline are consistently underestimated; the method's inabilty to reproduce an oscillating flame undergoing self-excited thermo-acoustic instabilities serves as a possible explanation for the underestimation. Franzelli et al. (2012) have shown significant improvements of the RMS temperature results close to the centreline by resolving flame oscillation in a previous LES of the same combustor. Despite this shortcoming, an accurate reproduction of the RMS temperature profiles away from the centreline can be determined. Radial profiles of the mean and RMS CO_2 mass fraction, depicted on the left-hand side of Fig. 5, show very similar trends supporting the aforementioned findings.

The instantaneous relation between temperature and mixture fraction is visualised on the right-hand side of Fig. 5 at four axial locations in order to analyse the numerically predicted thermochemistry. Each experimental scatter represents one single-shot laser Raman scattering measurement taken at different radial positions over time and all LES scatters were obtained at identical locations in the chamber. A solid line indicates the adiabatic flame temperature and the global mixture fraction is $Z_{glob} = 0.0391$. The temperature distribution at h_6 suggests that the assumed inlet temperature of 320 K is suitable to recreate experimental preheating of the mixture.

In terms of the mixture fraction distributions, experimental extreme values of about $Z_{min} \approx 0.015$ and $Z_{max} \approx 0.08$ can be observed. It becomes clear that the LES does not reproduce such a wide range of mixture fraction values but instead predicts a higher degree of premixing. The expanded experimental distribution is likely to be caused by the occurrence of thermo-acoustic instabilities periodically varying the amount of fuel in the mixture, as observed experimentally (Meier et al. 2007) and numerically (Franzelli et al. 2012). Furthermore, four stochastic fields in the calculation of the subgrid PDF evolution equation may not be enough to sufficiently account for the influence of the subgrid scale contributions. Previous findings by Mustata et al. (2006) and Jones and Navarro-Martinez (2007) suggest that eight stochastic fields provide a reasonable compromise between prediction accuracy and computational costs. A similar analysis with one stochastic field (not shown here) revealed an even narrower mixture fraction distribution representing a more homogeneous mixture. This is due to the micro-mixing and Wiener process terms being neglected in the formulation of the Eulerian stochastic field method when only one stochastic field is utilised.

Finally, looking at the evolution of the simulated temperature-mixture fraction distribution with downstream location, the shortened flame length determined from the mean temperature and CO_2 mass fraction results as well as the OH images can be observed once again. Unlike the experimental findings at axial position h_6, only a small amount of scatters is still located within the fresh gas region below approximately 400 K. At h_{15}, all of the scatters have moved up into either the reaction zone with intermediate temperatures or the fully burnt region close to the theoretical adiabatic flame temperature. Nevertheless, the overall instantaneous temperature-

mixture fraction relation matches experimental results including a reasonably estimated mixture fraction distribution.

5 Conclusions

The Eulerian subgrid PDF combustion model has been successfully applied to account for turbulence-chemistry interactions in the LES of a gas turbine model combustor for two different operating conditions. Time-averaged results of the temperature and major species mass fractions were overall in good agreement with measurement data demonstrating the capabilities of the subgrid PDF approach. An excellent reproduction of the velocity field was achieved supporting the applicability of the solver with a dynamic subgrid turbulence model to highly swirling flows. Similar to previous numerical studies of this particular combustor, heat loss in the experiments was found to be the source of local temperature overestimation towards the combustion chamber walls. The implementation of non-adiabatic walls can thus be identified as a scope for ensuing work. Furthermore it has to be noted, that both the flame length and width were slightly under predicted compared to experimental measurements. This may be attributed to a higher degree of premixing in the simulations caused by two potential factors. First, the utilisation of four stochastic fields in the calculation of the subgrid PDF evolution equation - subsequent simulations with a larger number of stochastic fields will show if further improvement of the results can be achieved. Second, the solver's low-Mach-number formulation prohibits any modulation of the local mixture fraction due to thermo-acoustic instabilities, which might additionally be the cause for underestimated scalar fluctuations near the combustor centreline. The computed thermochemical properties were finally analysed based on the instantaneous temperature-mixture fraction relation providing satisfactory agreement with measurement data. In summary, the employed LES method has been validated for partially premixed combustion in a complex geometry. All results were obtained without any adjustments to the model constants underlining the method's robustness in the simulation of turbulent reacting flow problems. A future extension of the method to fully compressible flow may reproduce thermo-acoustic instabilities observed in the experiments.

Acknowledgements

This work was supported by the Engineering and Physical Sciences Research Council (EPSRC) through the UK Consortium on Turbulent Reacting Flow (UKCTRF) and used the ARCHER UK National Supercomputing Service (http://www.archer.ac.uk). The authors are also grateful to SIEMENS Industrial Turbomachinery Ltd. for their financial support.

References

Barlow, R. S., Karpetis, A. N., Frank, J. H. and Chen, J. Y. 2001. Scalar profiles and NO formation in laminar opposed-flow partially premixed methane/air flames. *Combust. Flame*, **127**(3), 2102–2118.

Brauner, T., Jones, W. P. and Marquis, A. J. 2016. LES of the Cambridge stratified swirl burner using a sub-grid pdf approach. *Flow, Turbul. Combust.*, **96**(4), 965–985.

Bulat, G., Jones, W. P. and Marquis, A. J. 2013. Large eddy simulation of an industrial gas-turbine combustion chamber using the sub-grid PDF method. *Proc. Combust. Inst.*, **34**(2), 3155–3164.

Bulat, G., Jones, W. P. and Marquis, A. J. 2014. NO and CO formation in an industrial gas-turbine combustion chamber using LES with the Eulerian sub-grid PDF method. *Combust. Flame*, **161**(7), 1804–1825.

Caux-Brisebois, V., Steinberg, A. M., Arndt, C. M. and Meier, W. 2014. Thermo-acoustic velocity coupling in a swirl stabilized gas turbine model combustor. *Combust. Flame*, **161**(12), 3166–3180.

Dopazo, C. and O'Brien, E. E. 1974. Functional formulation of nonisothermal turbulent reactive flows. *Phys. Fluids*, **17**(11), 1968–1975.

Fiorina, B., Vicquelin, R., Auzillon, P., Darabiha, N., Gicquel, O. and Veynante, D. 2010. A filtered tabulated chemistry model for LES of premixed combustion. *Combust. Flame*, **157**(3), 465–475.

Franzelli, B., Riber, E., Gicquel, L. Y. M. and Poinsot, T. 2012. Large eddy simulation of com-

bustion instabilities in a lean partially premixed swirled flame. *Combust. Flame*, **159**(2), 621–637.

Gallot-Lavallée, S. and Jones, W. P. 2016. Large eddy simulation of spray auto-ignition under EGR conditions. *Flow, Turbul. Combust.*, **96**(2), 513–534.

Galpin, J., Naudin, A., Vervisch, L., Angelberger, C., Colin, O. and Domingo, P. 2008. Large-eddy simulation of a fuel-lean premixed turbulent swirl-burner. *Combust. Flame*, **155**(1-2), 247–266.

Gao, F. and O'Brien, E. E. 1993. A large-eddy simulation scheme for turbulent reacting flows. *Phys. Fluids A*, **5**(6), 1282–1284.

Jones, W. P., Marquis, A. J. and Noh, D. 2015. LES of a methanol spray flame with a stochastic sub-grid model. *Proc. Combust. Inst.*, **35**(2), 1685–1691.

Jones, W. P. and Navarro-Martinez, S. 2007. Large eddy simulation of autoignition with a subgrid probability density function method. *Combust. Flame*, **150**(3), 170–187.

Jones, W. P. and Prasad, V. N. 2010. Large eddy simulation of the Sandia flame series (D-F) using the Eulerian stochastic field method. *Combust. Flame*, **157**(9), 1621–1636.

Jones, W. P. and Prasad, V. N. 2011. LES-pdf simulation of a spark ignited turbulent methane jet. *Proc. Combust. Inst.*, **33**(1), 1355–1363.

Lecocq, G., Richard, S., Colin, O. and Vervisch, L. 2011. Hybrid presumed pdf and flame surface density approaches for large-eddy simulation of premixed turbulent combustion. Part 1: Formalism and simulation of a quasi-steady burner.. *Combust. Flame*, **158**(6), 1201–1214.

Meier, W., Weigand, P., Duan, X. R. and Giezendanner-Thoben, R. 2007. Detailed characterization of the dynamics of thermoacoustic pulsations in a lean premixed swirl flame. *Combust. Flame*, **150**(1-2), 2–26.

Mercier, R., Moureau, V., Veynante, D. and Fiorina, B. 2015. LES of turbulent combustion: On the consistency between flame and flow filter scales. *Proc. Combust. Inst.*, **35**(2), 1359–1366.

Moureau, V., Domingo, P. and Vervisch, L. 2011. From large-eddy simulation to direct numerical simulation of a lean premixed swirl flame: Filtered laminar flame-PDF modeling. *Combust. Flame*, **158**(7), 1340–1357.

Mustata, R., Valiño, L., Jiménez, C., Jones, W. P. and Bondi, S. 2006. A probability density

function Eulerian Monte Carlo field method for large eddy simulations: Application to a turbulent piloted methane/air diffusion flame (Sandia D). *Combust. Flame*, **145**(1-2), 88–104.

Oberleithner, K., Stöhr, M., Im, S. H., Arndt, C. M. and Steinberg, A. M. 2015. Formation and flame-induced suppression of the precessing vortex core in a swirl combustor: Experiments and linear stability analysis. *Combust. Flame*, **162**(8), 3100–3114.

Piomelli, U. and Liu, J. 1995. Large-eddy simulation of rotating channel flows using a localized dynamic model. *Phys. Fluids*, **7**(4), 839–848.

Pitsch, H. 2006. Large-eddy simulation of turbulent combustion. *Annu. Rev. Fluid Mech.*, **38**(1), 453–482.

Poinsot, T. and Veynante, D. 2005. *Theoretical and numerical combustion*, 2nd ed., RT Edwards, Inc., Philadelphia, PA

Roux, S., Lartigue, G., Poinsot, T., Meier, U. and Bérat, C. 2005. Studies of mean and unsteady flow in a swirled combustor using experiments, acoustic analysis, and large eddy simulations. *Combust. Flame*, **141**(1-2), 40–54.

Sabel'nikov, V. and Soulard, O 2005. Rapidly decorrelating velocity-field model as a tool for solving one-point Fokker-Planck equations for probability density functions of turbulent reactive scalars. *Phys. Rev. E*, **72**(1), 1–22.

Schmidt, H. and Schumann, U. 1989. Coherent structure of the convective boundary layer derived from large-eddy simulations. *J. Fluid Mech.*, **200**, 511–562.

Smagorinsky, J. 1963. General circulation experiments with the primitive equations. *Mon. Weather Rev.*, **91**(3), 99–164.

Steinberg, A. M., Arndt, C. M. and Meier, W. 2013. Parametric study of vortex structures and their dynamics in swirl-stabilized combustion. *Proc. Combust. Inst.*, **34**(2), 3117–3125.

Stöhr, M., Yin, Z. and Meier, W. 2017. Interaction between velocity fluctuations and equivalence ratio fluctuations during thermoacoustic oscillations in a partially premixed swirl combustor. *Proc. Combust. Inst.*, **36**(3), 3907–3915.

Sung, C. J., Law, C. K. and Chen, J. Y. 2001. Augmented reduced mechanisms for NO emission in methane oxidation. *Combust. Flame*, **125**(1-2), 906–919.

Valiño, L. 1998. A field Monte Carlo formulation for calculating the probability density function of a single scalar in a turbulent flow. *Flow, Turbul. Combust.*, **60**(2), 157–172.

Veynante, D. and Moureau, V. 2015. Analysis of dynamic models for large eddy simulations of turbulent premixed combustion. *Combust. Flame*, **162**(12), 4622–4642.

Volpiani, P. S., Schmitt, T. and Veynante, D. 2017. Large eddy simulation of a turbulent swirling premixed flame coupling the TFLES model with a dynamic wrinkling formulation. *Combust. Flame*, **180**, 124–135.

Wang, P., Fröhlich, J., Maas, U., He, Z. and Wang, C. 2016. A detailed comparison of two subgrid scale combustion models via large eddy simulation of the PRECCINSTA gas turbine model combustor. *Combust. Flame*, **164**, 329–345.

Yin, Z., Nau, P. and Meier, W. 2017. Responses of combustor surface temperature to flame shape transitions in a turbulent bi-stable swirl flame. *Exp. Therm. Fluid Sci.*, **82**, 50–57.

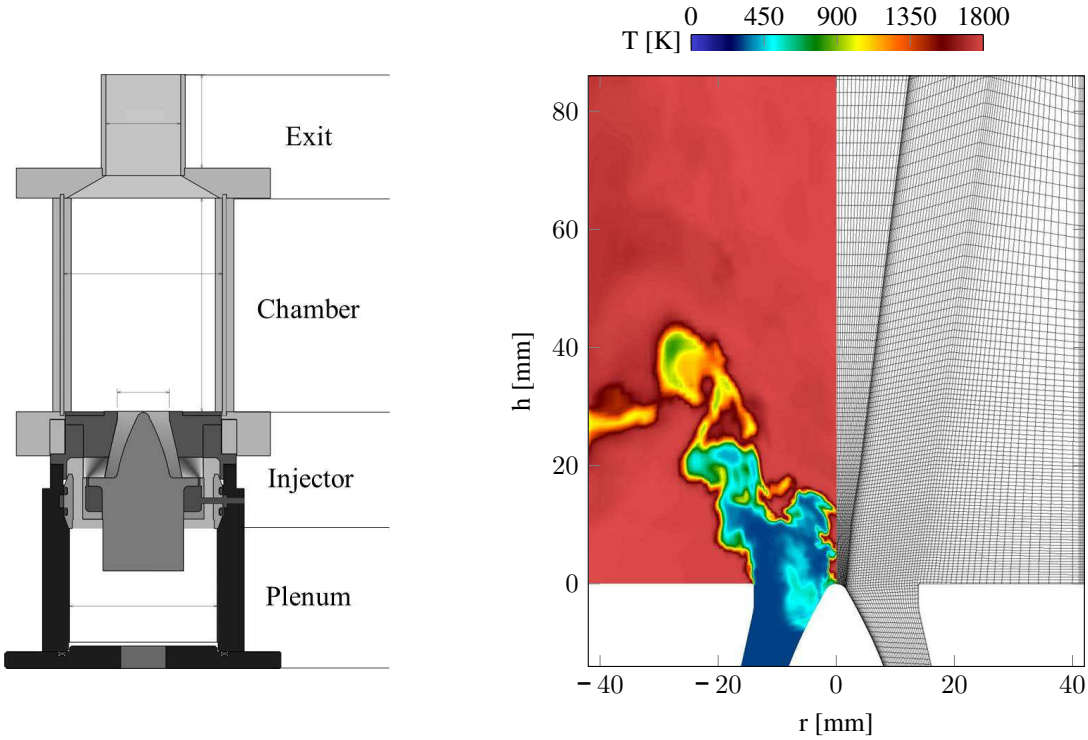

Figure 1. Schematic of the PRECCINSTA combustor (left) and snapshot of an instantaneous LES temperature field with a close-up of the computational mesh (right).

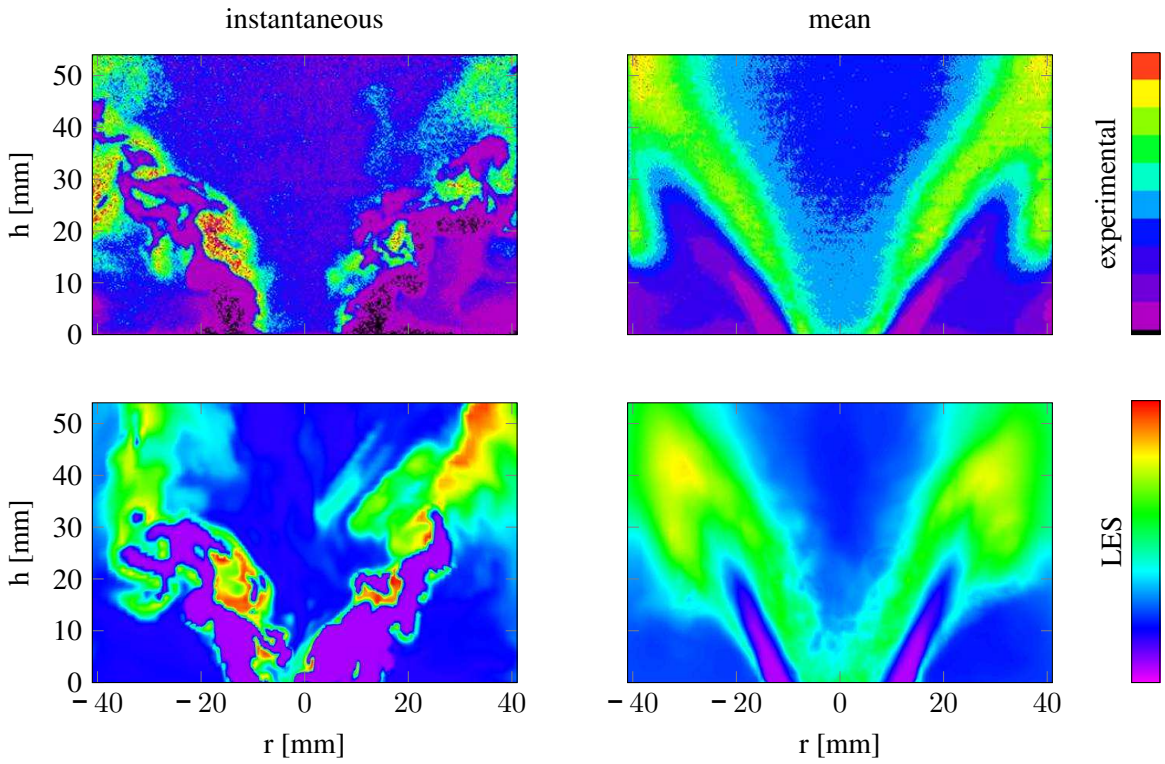

Figure 2. Comparison of the instantaneous (left) and mean (right) flame structure based on experimental OH-LIF measurements (top) and LES snapshots of the OH mass fraction (bottom). Note that the LES colour scale had to be approximated since the measurements are qualitative only.

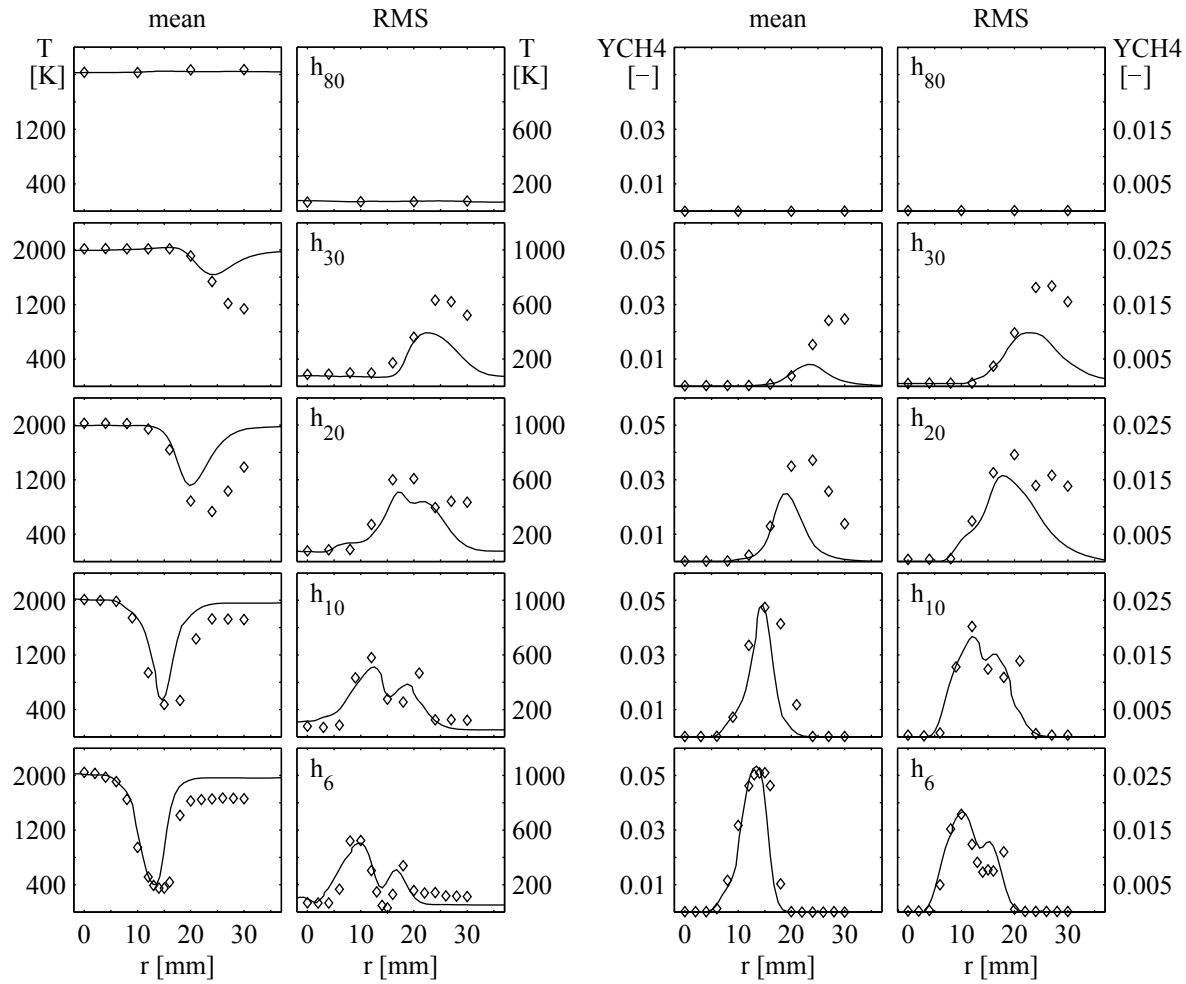

Figure 3. Radial profiles of both the mean and RMS temperature (left) and CH_4 mass fraction (right) for the 'quiet' flame case obtained from experiments (◇) and LES (−) at axial locations h = 6, 10, 20, 30, 80 mm.

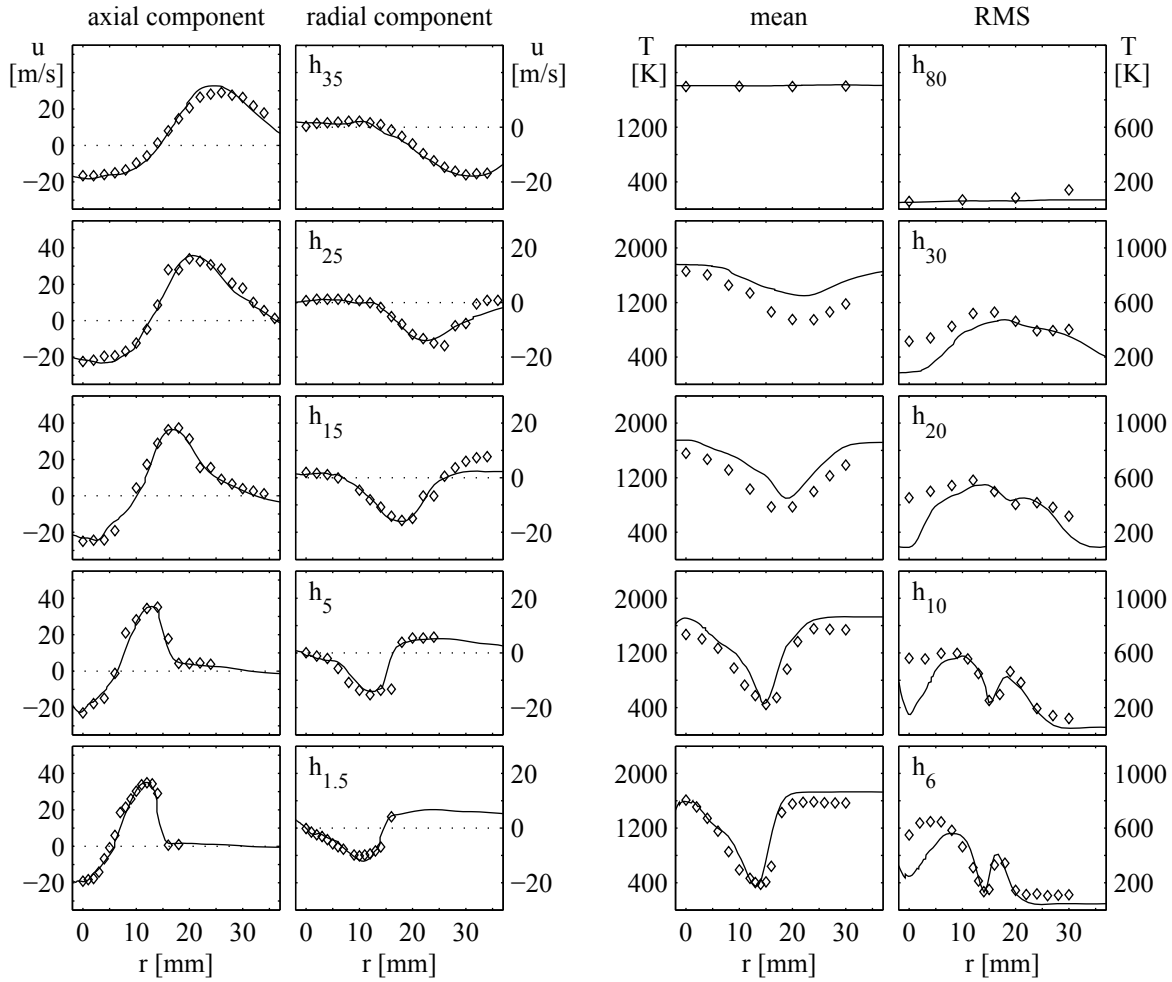

Figure 4. Radial profiles of the mean axial and radial velocity component (left) and the mean and RMS temperature (right) for the oscillating flame case obtained from experiments (◇) and LES (−) at axial locations h = 6, 10, 20, 30, 80 mm.

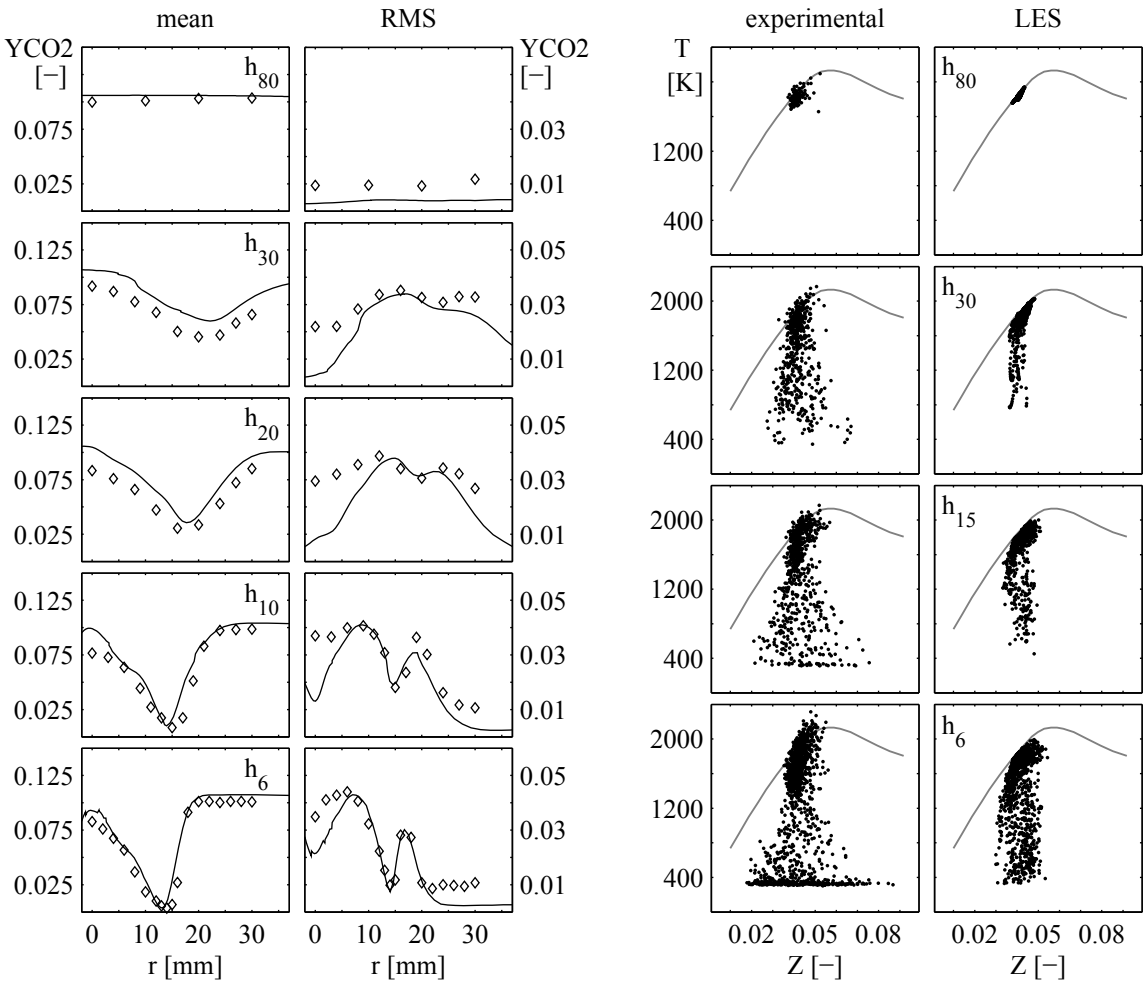

Figure 5. Radial profiles of the mean and RMS CO_2 mass fraction obtained from experiments ($\diamond$) and LES ($-$) (left). Experimental and LES scatter plots of the instantaneous temperature versus mixture fraction (right). Results are shown for the oscillating flame case at axial locations h = 6, 10, 15, 20, 30, 80 mm.

Table 1. Summary of three experimentally investigated combustor operating conditions.

Case	1	2a	2b
Equiv. ratio	0.7	0.83	0.75
Flame behaviour	Oscillating	‘Quiet’	Subtly pulsating
Measurements	LDV, Raman, LIF	Raman, LIF	LDV

Table 2. Experimental measurement uncertainties for selected quantities (Meier et al. 2007).

Uncertainty	Velocity	Temperature	Mixture fraction	Mass fraction	
				CH_4	CO_2
Systematic	$<$0.5%	$\pm$3-4%	$\pm$3-4%	$+$5-9%	$\pm$3-5%
Statistical	$\pm$1.5-2%	$\pm$2.5%	$\pm$1%	$\pm$1-3%	$\pm$7%

Table 3. 15-step ARM for methane involving 19 species (Sung et al. 2001).

Step	Reaction
1	$2H + 2OH \Leftrightarrow 2H_2 + O_2$
2	$2H \Leftrightarrow H_2$
3	$H + HO_2 \Leftrightarrow H_2 + O_2$
4	$H + H_2O_2 \Leftrightarrow H_2 + HO_2$
5	$OH + CH_3 \Leftrightarrow H_2 + CH_2O$
6	$H + CH_4 \Leftrightarrow H_2 + CH_3$
7	$H + OH + CO \Leftrightarrow H_2 + CO_2$
8	$CH_2O \Leftrightarrow H_2 + CO$
9	$O_2 + C_2H_2 \Leftrightarrow H_2 + 2CO$
10	$OH + C_2H_4 \Leftrightarrow H_2 + CH_3 + CO$
11	$C_2H_6 \Leftrightarrow H_2 + C_2H_4$
12	$H + OH \Leftrightarrow H_2O$
13	$2NO \Leftrightarrow O_2 + N_2$
14	$H_2 + CO + NO \Leftrightarrow H + O_2 + HCN$
15	$3H + H_2O + NH_3 \Leftrightarrow 4H_2 + NO$